JOURNAL OF PROPULSION AND POWER
Vol. 30, No. 6, November–December 2014

Role of a Conducting Vacuum Chamber in the Hall Effect Thruster Electrical Circuit

Jason D. Frieman,* Scott T. King,† and Mitchell L. R. Walker‡
Georgia Institute of Technology, Atlanta, Georgia 30332
Vadim Khayms§
Lockheed Martin Space Systems Company, Sunnyvale, California 94089
and
David King¶
Aerojet Rocketdyne Inc., Redmond, Washington 98052

DOI: 10.2514/1.B35308

The role of the electrically conductive vacuum chamber wall in the completion of the discharge circuit of a Hall effect thruster is experimentally investigated. The Aerojet Rocketdyne T-140 laboratory-model Hall effect thruster, operating at a discharge voltage of 300 V, a discharge current of 5.16 A, and an anode flow rate of 5.80 mg/s, serves as a representative Hall effect thruster testbed. The nominal facility operating pressure during thruster firings is 4.9×10^{-6} torr, corrected for xenon. Two 0.91×0.91 m, square aluminum plates are placed adjacent to, but electrically isolated from, the walls of the stainless-steel vacuum chamber at two locations with respect to the center of the thruster exit plane: 4.3 m axially downstream along the thruster centerline and 2.3 m radially outward centered on the exit plane. The plates are configured in three distinct electrical configurations with corresponding measurements: 1) electrically grounded plates with measurements of currents to ground, 2) electrically isolated plates with measurements of floating voltages, and 3) isolated but electrically connected plates with measurements of the current conducted between them. The measurements are all taken simultaneously, with the discharge current oscillations of the thruster at a sampling frequency of 100 MHz. Measurements of the current conducted to ground in the electrically grounded configuration reveal that the axial and radial plates collect ion currents that are 13.6 and 10.7% of the discharge current, respectively; the collected current is coupled to the discharge current oscillations but is smaller in magnitude and phase delayed. In the electrically connected-plate configuration, 5.5% of the average discharge current is observed to flow from the axial plate to the radial plate, driven by a floating voltage difference of 7.6 V; this current is uncorrelated in time with the discharge current oscillations. These results indicate that the vacuum chamber conducts current and is a recombination site for a significant number of plume ions during Hall effect thruster operation.

Nomenclature

I	=	current, A
P_b	=	vacuum chamber base pressure, torr
P_c	=	corrected vacuum chamber background pressure, torr
P_i	=	indicated vacuum chamber background pressure, torr
V	=	voltage, V
V_{c-g}	=	cathode-to-ground voltage, V
V_D	=	discharge voltage, V
V_p	=	plasma potential with respect to ground, V
V_{pa}	=	axial plate voltage with respect to ground, V
V_{pr}	=	radial plate voltage with respect to ground, V
ΔV	=	acceleration voltage, V
ΔV_{cath}	=	cathode coupling voltage, V

Received 21 January 2014; revision received 4 June 2014; accepted for publication 6 June 2014; published online 12 September 2014.

*Graduate Research Assistant, Aerospace Engineering, High-Power Electric Propulsion Laboratory; jfrieman3@gatech.edu. Student Member AIAA.

†Graduate Research Assistant, Aerospace Engineering, High-Power Electric Propulsion Laboratory; scott.king@gatech.edu. Student Member AIAA.

‡Associate Professor, Aerospace Engineering, High-Power Electric Propulsion Laboratory; mitchell.walker@ae.gatech.edu. Associate Fellow AIAA.

§Electric Propulsion Architect; vadim.khayms@lmco.com. Member AIAA.

¶Technical Fellow, Engineering; david.king@rocket.com. Member AIAA.

I. Introduction

DUE to the high specific impulse, thrust efficiency, and thrust density provided by Hall effect thrusters (HETs), a number of commercial and government Earth-orbiting satellite missions have identified them as an appealing choice for use as the primary onboard propulsion system. In addition to the mass savings offered by these performance attributes, developments in in-space power and the growing western flight heritage portfolio of HETs have also increasingly made them prime candidates for more ambitious deep-space missions, including the recently proposed Asteroid Retrieval Mission [1].

The growth in interest and popularity of these devices has caused a corresponding proliferation of facilities conducting HET research and testing. Despite the similarities among the devices tested and measurements recorded at each of these facilities, the wide range of facility geometries, sizes, materials, and base pressures makes it difficult for researchers to compare datasets without the inclusion of facility-dependent corrections [2]. It is therefore necessary to develop an understanding of how to quantify facility effects on HET operation and data collection so that facility-dependent testing artifacts can be corrected for and a facility-independent understanding of the actual device performance can be achieved.

Although several investigations into facility effects exist in the literature, most focus on the role of facility backpressure on data collection and device operation. Previous studies have shown that increases in facility pressure result in artificial increases in device thrust and efficiency due to neutral ingestion or entrainment [3–9]. Work has also been conducted linking background pressure to parasitic facility effects caused by resonant charge exchange (CEX) collisions. Specifically, it has been shown that higher facility pressures lead to increased CEX collisions, which, in turn, introduce additional plume components and artificially increase the ion current density measured by Faraday probes in the extremities of the HET

plume [8,10–12]. Azziz suggests that the relationship between current density and background pressure is linear for all angular positions in the HET plume [13]. This body of experimental evidence on pressure effects is ultimately focused on the development of a process by which to calibrate any vacuum facility in terms of pressure [12].

Despite the fact that HET test facilities are almost ubiquitously metallic, limited effort has thus far been expended to examine the effects of chamber conductance on the discharge circuit of the HET. Prior efforts have analyzed the propagation of standing wave noise in metallic chambers for electromagnetic interference (EMI) testing; however, such work has not been extended to include the role of the chamber in the actual HET system circuit [2,3].

This paper experimentally investigates the role of a conductive facility on the discharge circuit of a HET. A representative facility testbed with controllable wall bias is created by placing two large square aluminum plates adjacent to, but electrically isolated from, the walls of the vacuum test facility, both axially downstream and radially outward from the exit plane of the Aerojet Rocketdyne T-140 HET. To assess the impact of the chamber's electrical configuration on the plasma discharge, measurements of the current conducted through the plates as well as the voltage to which the plates are biased are taken as the plates are electrically isolated, connected, and grounded.

II. Experimental Setup

A. Vacuum Facility

All experiments were performed in Vacuum Test Facility 2 (VTF-2) at the Georgia Institute of Technology High-Power Electric Propulsion Laboratory (HPEPL). A schematic of this facility is shown in Fig. 1. VTF-2 is a stainless-steel chamber measuring 9.2 m in length and 4.9 m in diameter. VTF-2 is evacuated to rough vacuum using one 495 ft^3/min rotary-vane pump and one 3800 ft^3/min blower. High vacuum is achieved using 10 liquid-nitrogen-cooled CVI TMI-1200i reentrant cryopumps. The cryopump shrouds are fed using the Stirling Cryogenics SPC-8 RL special closed-loop nitrogen liquefaction system detailed by Kieckhafer and Walker [14]. The facility has a combined nominal pumping speed of 350,000 l/s on xenon and can achieve a base pressure of 1.9×10^{-9} torr with a nominal operating pressure for this work of 4.9×10^{-6} torr, corrected for xenon. Pressure in VTF-2 is monitored using an Agilent BA 571 hot-filament ionization gauge controlled by an Agilent XGS-600 gauge controller. The corrected pressure, P_c, is found by relating the indicated pressure, P_i, and the vacuum chamber base pressure, P_b, to a gas-specific constant using the following equation [15]:

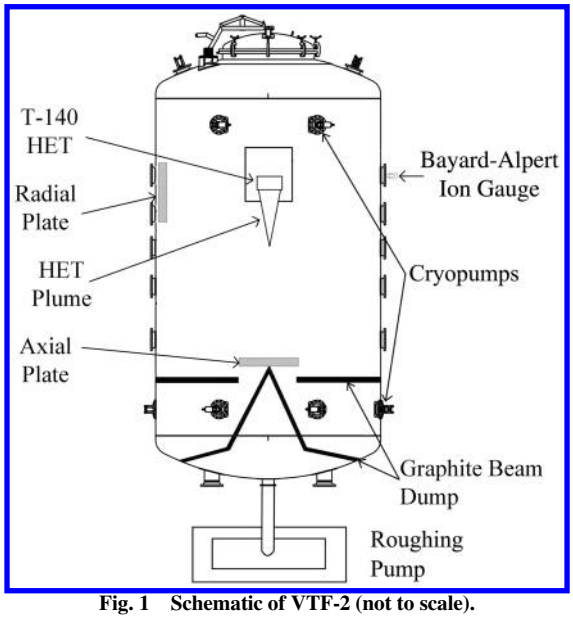

Fig. 1 Schematic of VTF-2 (not to scale).

$$P_c = \left[\frac{P_i - P_b}{2.87}\right] + P_b \tag{1}$$

B. T-140 HET

All experiments detailed in this work were performed using the Aerojet Rocketdyne T-140 HET originally developed by Space Power, Inc., in collaboration with the Keldysh Research Center and Matra Marconi Space [16]. The T-140 HET is a laboratory-model HET that has a discharge channel made of M26-grade boron nitride with an outer diameter of 143 mm. The performance of the T-140 has been extensively mapped by prior investigations [16].

An Electric Propulsion Laboratory Hollow Cathode Plasma Electron Emitter 500-series cathode was located at the "12 o'clock" position of the thruster. The orifice of the cathode was located approximately 2.54 cm downstream from the thruster exit plane and 18.1 cm radially outward from the thruster centerline. The magnetic field strength at the orifice was approximately 30 G at this location. The cathode flow rate was set to a constant 0.59 mg/s, and the declination was fixed at 55 deg with respect to the thruster centerline.

The magnetic circuit configuration of the T-140 HET (two concentric coils centered on the thruster centerline) restricts the position of the magnetic field separatrix to the thruster centerline and precludes the T-140 HET from exhibiting the off-centerline separatrix surfaces in HETs with magnetic coils centered off axis [17,18]. This magnetic field topology eliminates any concerns from this work about the changing nature of the near-field plume properties and cathode coupling as a function of cathode position relative to the absent off-centerline separatrix surface [17].

The T-140 HET discharge was controlled using a 10 kW Regatron TopCon Quadro TC.P.20.1000.480.SHMI power supply. All other thruster components were powered using TDK-Lambda GEN60-25 power supplies. TDK-Lambda GEN150-10 and GEN40-38 power supplies were used for the cathode keeper and heater, respectively. All electrical connections entered VTF-2 through separate feedthroughs to eliminate potential EMI concerns. The thruster discharge supply was connected to a discharge filter consisting of a 95 μF capacitor and 1.3 Ω resistor in order to prevent oscillations over 1.4 kHz in the discharge current from reaching the discharge supply. The discharge current oscillations of the T-140 HET were recorded using a FW Bell IHA-25 open-loop Hall sensor connected to a Tektronix TDS3034B oscilloscope. The uncertainty and bandwidth of the Hall sensor are $\pm 2.5\%$ and 500 kHz, respectively; for the oscilloscope, they are $\pm 2\%$ and 300 MHz. The cathode-to-ground voltage and the anode-to-cathode voltage were measured using Fluke 83V multimeters, which have an uncertainty of $\pm 0.1\%$.

High-purity (99.9995%) xenon propellant was supplied to the thruster and cathode using stainless-steel lines metered with MKS 1179A mass flow controllers. The controllers were calibrated before each test by measuring gas pressure and temperature as a function of time in a known control volume. The mass flow controllers have an uncertainty of ± 0.03 mg/s (5.1%) for the cathode flow and ± 0.12 mg/s (2%) for the anode flow [19,20].

C. Configuration of Plates

To simulate a metallic facility with controllable wall bias, two 0.91 m × 0.91 m × 0.16-cm-thick square aluminum plates were mounted adjacent to, but electrically isolated from, the walls of the vacuum test facility. The axial plate was located 4.3 m downstream from the exit plane of the thruster. The radial plate was located 2.3 m radially outward from the thruster centerline and was centered on the exit plane of the T-140 HET. Figure 1 shows the physical location of the plates with respect to the T-140 HET.

Figure 2 shows each of the four plate electrical configurations used in this test. In all four cases, the electrical connection to the plates was made using a RG-58 coaxial cable with a grounded shield that passed through a Bayonet Neill-Concelman (BNC) feedthrough into the chamber. This transmission line is similar in style to those previously used to study discharge oscillations in HETs [21,22].

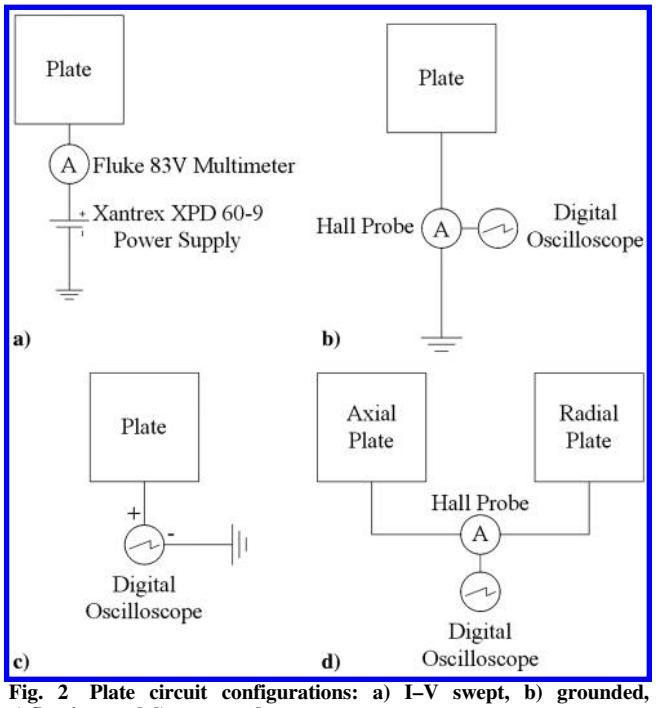

Fig. 2 Plate circuit configurations: a) I–V swept, b) grounded, c) floating, and d) connected.

In configuration A (I-V-swept), each of the plates was effectively used as a large planar Langmuir probe [23,24]. The bias voltage was controlled using a Xantrex XPD 60-9 power supply, and the plate current was measured using a Fluke 83V multimeter. In configuration B (grounded), each plate was directly connected to chamber ground with the current conducted between each plate and ground measured with a FW Bell IHA-100 open-loop Hall sensor (±2.5% uncertainty and 500 kHz bandwidth) connected to a Tektronix TDS3034B oscilloscope; the plate currents and discharge current were measured simultaneously at a sampling frequency of 100 MHz to eliminate any potential phasing effects that could result from asynchronous sampling. In configuration C (floating), the plates were electrically isolated, and the floating voltage was measured directly using a RG-58 coaxial cable connected via BNC to the Tektronix oscilloscope; these voltage measurements were also taken simultaneously with measurements of the T-140 HET discharge current oscillations at a sampling frequency of 100 MHz. In configurations A, B, and C, the plate not actively being biased was floating. In configuration D (connected), the plates were connected to each other instead of to ground, and the current conducted between the two plates was measured with a FW Bell IHA-100 open-loop Hall sensor connected to a Tektronix TDS3034B oscilloscope; the current conducted between the two plates and the discharge current were measured simultaneously at a sampling frequency of 100 MHz.

III. Results

All data were collected with the T-140 HET operating at a discharge voltage of 300 V, a discharge power of 1.5 kW, an anode xenon flow rate of 5.80 mg/s, and a cathode xenon flow rate of 0.59 mg/s. The thruster voltage, inner and outer magnet currents, anode mass flow rate, and cathode mass flow rate were held constant for all test configurations. The thruster was run through a 3 h conditioning cycle before data collection in order to allow the thruster to approach thermal equilibrium.

A. Configuration A: I-V-Swept Plates

Figures 3a and 3b show the current collected by the axial and radial plates, respectively, along with the corresponding T-140 HET cathode-to-ground voltage as a function of imposed plate bias voltage in the swept-plate configuration shown in Fig. 2a. Despite the large size of the plates, both I–V sweeps show the three distinct regions (i.e., ion saturation, transition, and electron saturation) typical of Langmuir probe characteristics, with the features appearing more pronounced for the axial plate [23,24]. In addition to Langmuir probe behavior, the I–V sweeps in Figs. 3a and 3b reveal a noticeable coupling between the plate bias voltage and the cathode-to-ground voltage of the T-140 HET. For both the axial and radial plates, once the bias voltage becomes sufficient to begin repelling ions and the I–V characteristic exits the ion saturation region, the cathode-to-ground voltage increases monotonically with bias voltage. The observed magnitude of this effect is stronger for the axial plate than for the radial plate.

B. Configuration B: Grounded Plates

Figures 4a and 4b show the discharge current oscillations and plate current measured by the axial and radial plates, respectively, in the grounded-plate configuration shown in Fig. 2b. In this configuration, the axial plate collected, on average, a current of −0.70 A, whereas the radial plate collected −0.55 A of current, which represents 13.6 and 10.7% of the discharge current, respectively. The sign of the current indicates that a net ion current was conducted from the plates to ground, thus causing electrons to flow from ground to the plate so as to recombine with the incident ions. The average discharge current is 5.16 A in both Figs. 4a and 4b.

Care must be taken when interpreting Fig. 4, as the bandwidth limitations of the employed Hall probe limits the frequency resolution of the data to 50 kHz and below. Thus, the intermittent

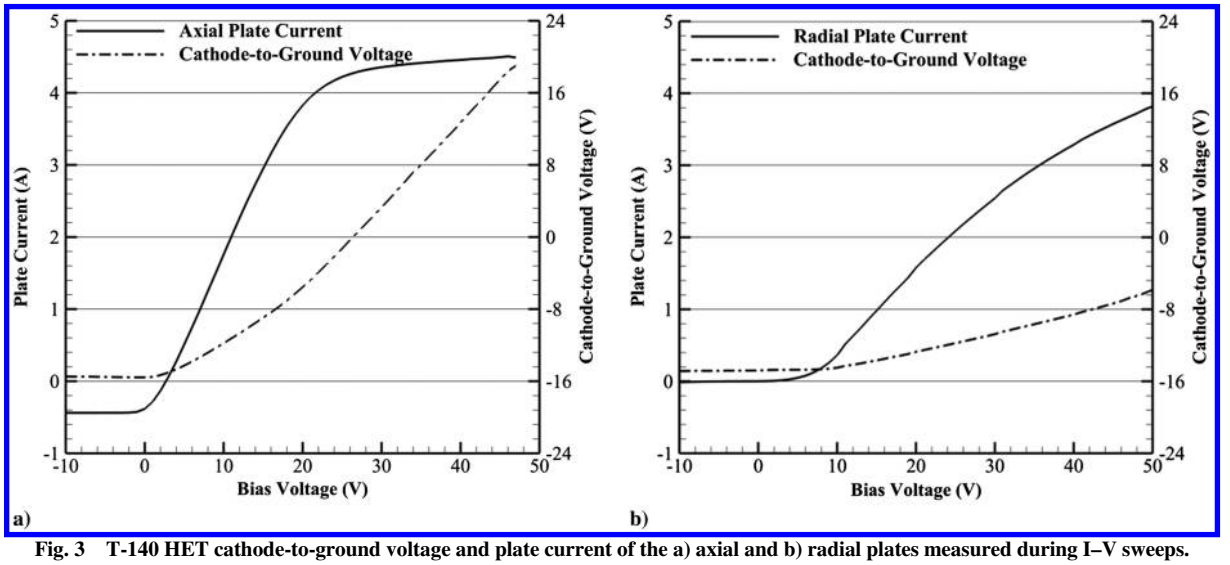

Fig. 3 T-140 HET cathode-to-ground voltage and plate current of the a) axial and b) radial plates measured during I–V sweeps.

high-frequency oscillations shown in Fig. 4b are likely sampling errors and should not be interpreted as significant or indicative of a variation in T-140 HET performance. A frequency analysis of the plate current was unable to isolate any signals in the 15–22 kHz band characteristic of the breathing mode of the thruster or in the other frequency bands up to the 50 kHz limit of the probe indicative of rotating spoke or gradient-induced oscillations [21,22,25–27]. It is expected that this result was, in part, due to resolution limitations with the data acquisition equipment: specifically, the high-frequency aliasing induced by the aforementioned bandwidth limitations of the Hall probe and resolution limitations induced by the bit limitations of the oscilloscope.

To remove the high-frequency aliasing, the plate current was passed through a moving average filter. The filtered plate current collected by the axial and radial plates is shown in Figs. 4c and 4d, respectively, along with the synchronous T-140 HET discharge current. Overall, the traces of the filtered collected axial plate current and the T-140 HET discharge current have the same waveform, but the axial plate current collects less current and has a phase-delayed waveform relative to the discharge current. This coupling between discharge current and filtered plate current is also present for the radial plate but with decreased current collection as compared to the axial plate.

C. Configuration C: Floating Plates

Figures 5a and 5b show the thruster discharge current oscillations and plate floating potential for the axial and radial plates, respectively, collected using the floating-plate configuration shown in Fig. 2c. Despite having nearly identical discharge current traces, Figs. 5a and 5b reveal that the floating potential axially downstream of and radially outward from the thruster are very different. The axial plate profile has an average floating potential of 2.4 V, whereas the radial plate has a lower average potential of −5.2 V; these results are consistent with those from the I–V sweeps shown in Figs. 3a and 3b. Unlike with the current collected in the grounded configuration, the floating voltage traces do not show a coupling to the discharge current oscillations but instead oscillate around a nearly constant mean.

D. Configuration D: Connected Plates

Figure 6 shows the thruster discharge oscillations and plate-to-plate current conducted for the connected-plate configuration shown in Fig. 2d. The average conducted plate-to-plate current was 0.29 A, which represents 5.5% of the average measured discharge current. The high-frequency bursts seen in the grounded-plate configuration are also apparent in Fig. 6a but should again be disregarded as sampling errors due to the limited bandwidth of the Hall probes.

As with the grounded-plate configuration, a moving average filter was applied to the plate-to-plate current to remove the high-frequency noise. The filtered plate-to-plate current is shown along with the synchronous discharge current in Fig. 6b. Unlike the grounded plates, the connected-plate current does not show a strong correlation with the discharge current.

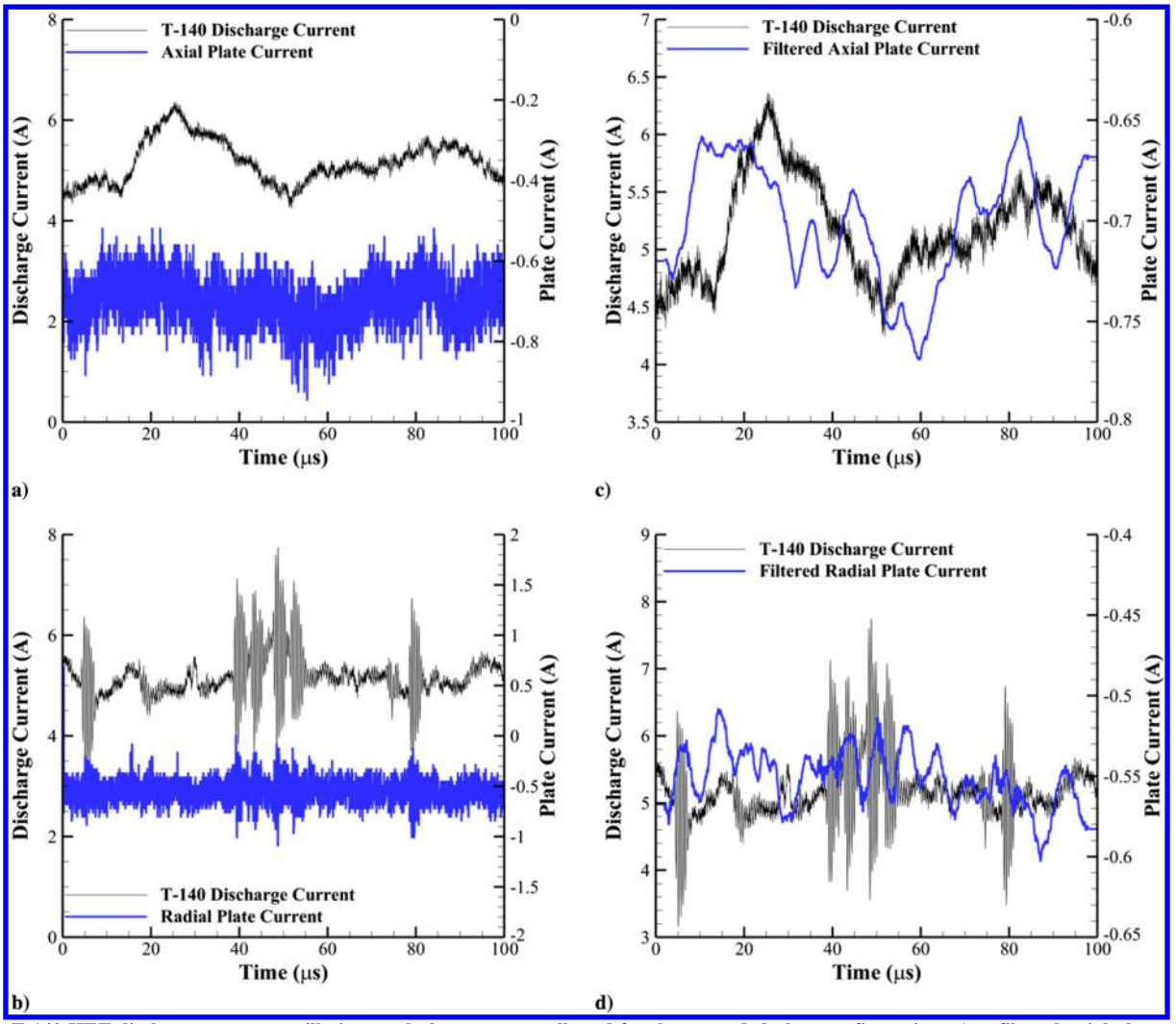

Fig. 4 T-140 HET discharge current oscillations and plate current collected for the grounded-plate configuration: a) unfiltered axial plate current, b) unfiltered radial plate current, c) moving-average filtered axial plate current, and d) moving-average filtered radial plate current.

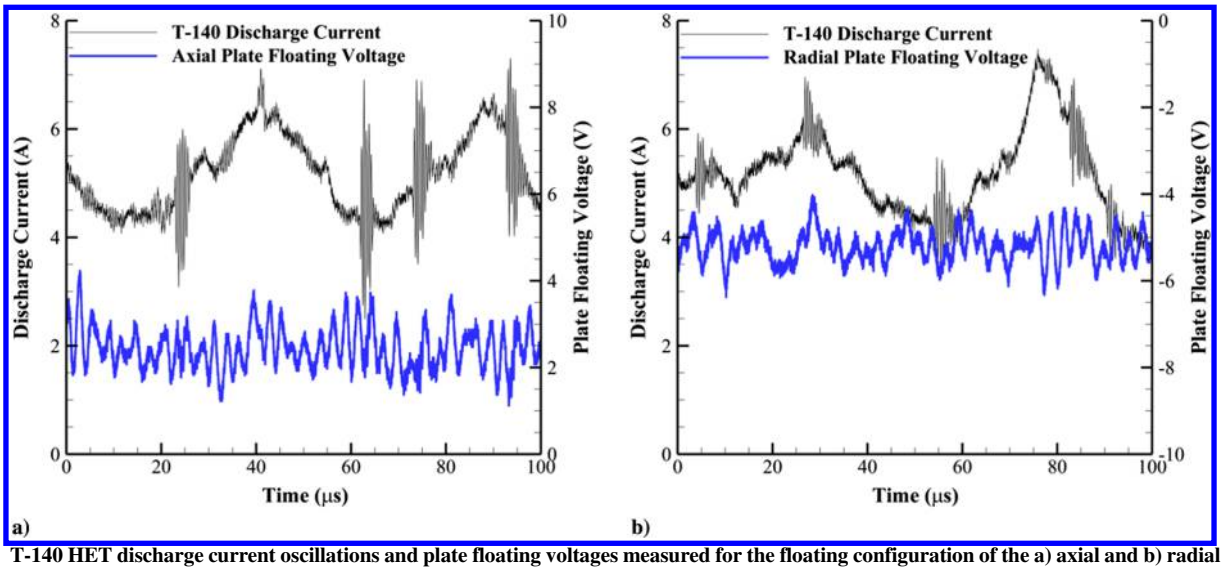

Fig. 5 T-140 HET discharge current oscillations and plate floating voltages measured for the floating configuration of the a) axial and b) radial plates.

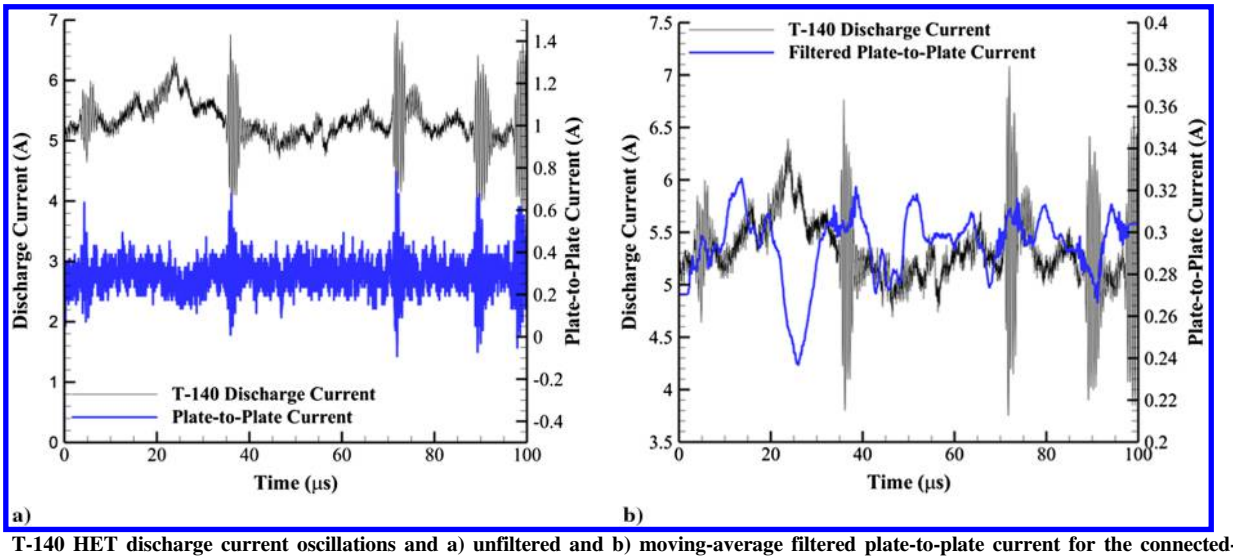

Fig. 6 T-140 HET discharge current oscillations and a) unfiltered and b) moving-average filtered plate-to-plate current for the connected-plate configuration.

IV. Discussion

A. Grounded-Plate Configuration

Before considering the physical processes governing the I–V characteristics from the swept-plate configuration, the nature of the HET plume impinging upon the grounded plates must first be discussed. The grounded-plate configuration shows that both the axial and radial plates collect current from the HET plume, with the axial plate collecting more current than the radial plate. This result is expected, since the HET plume is a conductive plasma and has line-of-sight impingement on the axial plate, whereas the positioning of the radial plate keeps it out of the line of sight of the collimated HET ion beam. Furthermore, the highest current density in the HET plume coincides with the HET centerline axis, and is thus directed toward the axial plate [28]. The nonzero current collected by both plates indicates that the ions in the HET plume have not completely recombined with the plume electrons by the time the ions reach the chamber walls; thus, the grounded wall acts as an alternate recombination pathway for those plume ions that reach the wall before undergoing recombination collisions with cathode electrons. This result is not unexpected, as the ion–electron recombination collision rates in a HET plume are sufficiently small in the near field to be neglected in plume models [29,30]. Since the ion recombination is therefore completed at the conducting vacuum facility wall, the potential of these surfaces will impact the plasma potential with respect to ground. This dependence is an artificial effect introduced by the presence of the vacuum facility and is expected to be absent on orbit. Furthermore, the completion of the recombination process at the wall, as well as the collection of a significant electron current by the radial plate, significantly alters the path of the electrons in the vacuum test facility. Instead of being forced to travel to the HET plume for collisional recombination, the electrons, instead, can travel to the facility wall to be conducted directly to ground. Thus, any process dependent upon the path of the electrons through the plasma (including plasma reactance and resistance) may be significantly different between facility operation and operation on orbit [17,31]. This change may need to be accounted for during ground testing. Finally, the completion of the recombination process at the facility walls could also result in the production of secondary ions due to the impact of the ions with the wall. However, the effect and creation of these secondaries was not measured or quantified for this work.

B. I–V-Swept Plates

The I–V sweeps from the swept-plate configuration shown in Fig. 3 reveal that the electrical potential of the facility, simulated by plate bias voltage, directly impacts the cathode-to-ground voltage of the HET. As shown in Fig. 3a, negative bias voltages and low positive bias voltages (i.e., less than 2 V on the axial plate and less than 10 V on the radial plate) do not affect the cathode-to-ground voltage. After this limit, however, the cathode-to-ground voltage increases as the plate bias increases. Figure 3a indicates that the axial plate cathode-

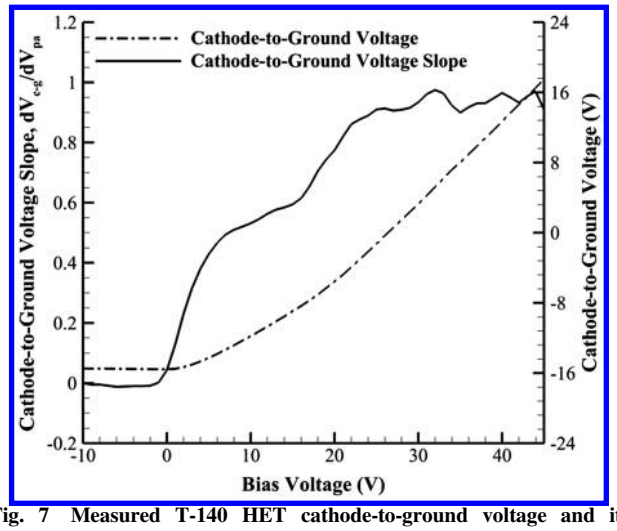

Fig. 7 Measured T-140 HET cathode-to-ground voltage and its derivative with respect to axial plate bias voltage as a function of bias voltage.

to-ground voltage has two nonzero linear sections: the first section at lower bias voltages has a moderate slope, whereas the second section at higher bias voltages has a greater slope. This trend is best seen in Fig. 7, which plots the derivative of the cathode-to-ground voltage, V_{c-g}, with respect to the applied axial plate bias voltage, V_{pa}, as a function of the bias voltage. This plot shows that the two linear sections in Fig. 3a correspond to slopes of approximately 0.55 and 0.98, respectively. This indicates that, as the axial plate bias voltage increases, there is a point at which the plate bias voltage and cathode-to-ground voltage rise at nearly a one-to-one ratio.

The observed relationship between cathode-to-ground voltage and the axial plate bias voltage is explained by sheath physics on the biased wall. Overall, the axial plate acts as a planar Langmuir probe and produces an I–V characteristic with the expected three distinct regions (i.e., ion saturation, transition, and electron saturation) [23,24]. However, in the analysis of Langmuir probes, it is often assumed that the probe geometry is sufficiently small that the probe bias does not affect the bulk plasma [23]. The size of the axial plate relative to the plasma sheath renders this assumption invalid for the present work, as the Debye length near the axial plate is approximately 70 μm. In previous experimental and computational work with large biased electrodes in contact with a plasma, it has been shown that increases in bias voltage cause a corresponding increase in plasma potential [32–34]. This relationship is identical to the form of the cathode-to-ground voltage curves shown in Fig. 3 and provides the physical explanation for the observed HET behavior [32].

At negative voltages and low positive voltages (i.e., less than 2 V), the axial plate acts as a planar Langmuir probe that has reached ion saturation. No change in cathode-to-ground voltage is observed in this regime because the plasma potential must remain sufficiently positive with respect to ground to keep the thermal electrons trapped within the bulk discharge to maintain quasi-neutrality. Further decreases in bias voltage will simply decrease electron flow to the surface but will not affect ion flow. Consequently, the plasma potential is prevented from continuously dropping with decreasing bias voltage, as the biasing does not also perturb the plasma density or electron temperature [33,34].

At axial plate bias voltages above approximately +2 V, the sheath begins to expand and collect additional electrons. As the bias is increased further, the electron flow to the surface also increases, thus leaving only the highest energy electrons confined in the bulk plasma. The corresponding drain of negative charge from the plasma pushes the plasma potential higher in order to maintain a quasi-neutral bulk plasma [34].

Once the bias voltage on the axial plate is high enough (i.e., around 30 V), the plate reaches the electron saturation limit. Further increases in the bias voltage do not increase the current collected by the plate because there are no additional electrons to collect from the plasma; all remaining electrons in the beam that have otherwise not undergone electron–ion recombination before reaching the axial plate are now being collected by it. Therefore, the plasma potential must respond to increases in bias voltage with a nearly one-to-one voltage increase, since the plasma cannot provide additional electrons yet must provide the same charge flux to maintain quasi-neutrality [33,34].

The response of the cathode-to-ground voltage is tied to that of the plasma potential by the coupling voltage of the cathode. The coupling voltage, ΔV_{cath}, is a loss term that is defined as the difference between the plasma potential and the cathode-to-ground voltage, and it indicates the resistance to electron transport between the cathode and HET anode [4,18,31]. The cathode in turn emits a flow of electrons equal to the discharge current. Since the ion beam current is constant across all plate biases, the electron current out of the cathode must also be a constant. Thus, an increase in plasma potential at high plate bias causes a corresponding increase in cathode-to-ground voltage in order to maintain a fixed coupling voltage and to provide a constant electron current from the cathode.

Since the steady increase in cathode-to-ground voltage with axial plate bias voltage is observed once nearly all of the plume electrons are collected, it is postulated that, if the entire chamber were biased in the same manner as the axial plate, the cathode-to-ground voltage would respond with a one-to-one voltage increase even at low positive bias voltages, because all of the plasma electrons would already be impinging on the chamber walls. A corresponding increase in the plasma potential would then result, since the chamber walls would not be able to collect additional electrons. Furthermore, previous studies have found that, so long as the surface area exposed to the plasma remains nearly constant, the effect of plate bias on plasma potential is independent of the shape of the electrode [32]. Thus, this same phenomenon is expected to occur in all chambers with dimensions shorter than several ion–electron recombination mean free paths, since not all ions will have recombined via collisional interactions in the plume before reaching the facility wall.

Biasing of the radial plate does not affect cathode-to-ground voltages until larger radial plate bias voltages are reached. Unlike the axial plate, the radial plate does not have plume plasma impinging directly upon it. Instead, the radial plate primarily interfaces with a less dense plasma composed of CEX ions and nonmagnetized cathode electrons, and thus does not have the direct line-of-sight conductive connection through the energetic plume ions. As a result, the applied voltage must be higher in order to draw a sufficient flux of electrons to cause an increase in cathode-to-ground voltage. However, once a sufficient flux of electrons is attracted to the plate, the same coupling to the cathode-to-ground voltage as with the axial plate is observed.

The net effect of the changing cathode-to-ground voltage and plate bias voltages on HET performance can be estimated using the acceleration voltage, ΔV, which is the potential across which the beam ions are accelerated. The acceleration voltage is a function of discharge voltage (V_D), cathode-to-ground voltage, V_{c-g}, and plasma potential, V_p, and it is defined using Eq. (2) [4]:

$$\Delta V = V_D - V_p + V_{c-g} \tag{2}$$

Note that, in Eq. (2), the signs of the voltages relative to ground must be included. The discharge voltage for this work is a constant for all plate bias voltages. Furthermore, as previously described, the difference between the cathode-to-ground voltage and plasma potential must also remain constant in order to maintain the required electron current to the plume. Thus, the acceleration voltage must also remain nearly constant with plate bias voltage.

This trend is shown qualitatively in Figs. 8a and 8b. Instead of changing the voltage difference between the anode and the bulk plasma, the increase in plate bias serves only to shift the potentials of the entire HET circuit upwards with respect to ground. Since the acceleration voltage determines the kinetic energy and generated thrust of the exhausted beam ions, the invariance in acceleration voltage with respect to plate bias also implies an invariance in thruster performance with respect to chamber bias. However, without plasma

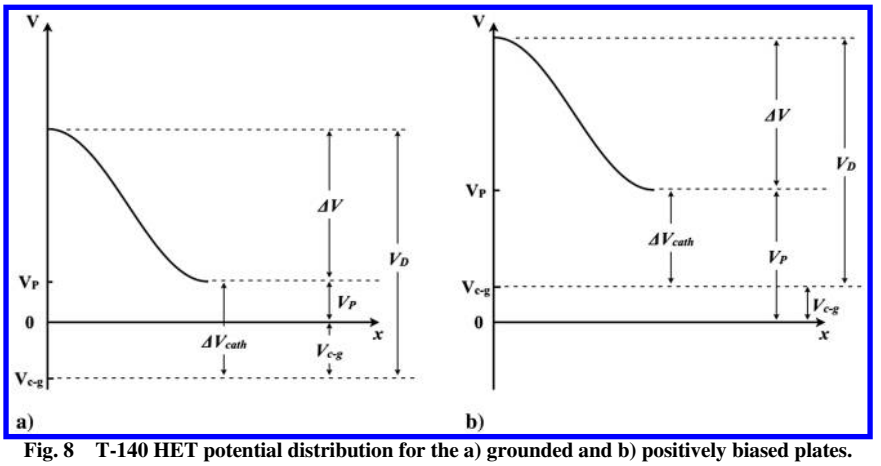

Fig. 8 T-140 HET potential distribution for the a) grounded and b) positively biased plates.

potential measurements and thrust data, the effect on HET performance cannot be fully quantified.

C. Floating-Plate and Connected-Plate Configurations

Both the floating-plate and connected-plate configurations provide additional insight into the electrical role of the chamber in the HET discharge circuit at lower bias voltages. The floating-plate configuration shows that the axial and radial plates floated to 2.4 and −5.2 V, respectively. The observed potential difference between the two floating plates is expected due to the spatial configuration of the plates and of the HET plume. As shown in Fig. 1, the axial plate is located downstream of the centerline of the T-140 HET. This placement subjects the axial plate to direct impingement from the densest region of HET plume ions, thus necessitating that the plate floating voltage increase in order to maintain an equal flux of ions and electrons to the surface of the plate [24]. The radial plate is not directly impinged upon by the energetic plume ions, as it is located in the angular wings of the HET plume. This plume location is characterized by a low current density (relative to the plume centerline) plasma composed primarily of slow CEX ions and electrons [8,10–12,28]. In this region, the electron mobility is unlikely to be constrained by magnetization due to the negligible magnetic field present, and there should be little to no radially directed, ion beam [35]. Thus, by virtue of their smaller mass, the electrons are the more mobile species in the near-plate region, and therefore the primary species impinging upon the radial plate [24]. This is confirmed by Fig. 3b, which shows that, for the radial plate, the floating potential lies within the ion saturation region; thus, in order to maintain equality of ion and electron flux to the surface, the radial plate must float at a potential that maximizes the collected ion current, a condition necessitated when the near-field electron impingement is much greater than that of the ions. Consequently the floating voltage of the radial plate is driven lower in order to maintain the net-zero current boundary condition necessitated by the floating surface [24].

The connected-plate configuration expands upon the results of the floating-plate configuration to indicate that the walls of the vacuum test facility also conduct current even if the walls are floating. The current flow through the walls of this simulated floating chamber acts to spatially redistribute the charge collected from the HET plume instead of simply providing a charge sink to ground, as was the case for the grounded-plate configuration. Although the combined plate surface area is only 2% of the total test facility wall area, 5.5% of the HET discharge current was observed to be conducted between the two floating plates. This result indicates that a significant amount of the HET current passes through the conducting chamber walls.

Applying a moving average filter to the current and voltage data from the grounded- and floating-plate configurations, respectively, removes the high-frequency noise from these signals and serves to better reveal the role played by the chamber walls of either a grounded or floating chamber. In the grounded-plate configuration, the oscillations observed in the discharge current also appear, although out of phase, in the waveform of the current conducted from each plate to ground. This result indicates that the discharge current is itself the forcing function to which the current conducted to ground from the plate must respond. In other words, the greater the discharge current, the greater the flux of ions that are recombined on the plate by sinking their charge to ground.

The observed attenuation of the plate-to-ground current relative to the discharge current oscillations in the grounded-plate arises from the divergence of the beam, which prevents the axial plate from collecting the full beam current. This attenuation is larger for the radial plate due to its spatial location outside of the line of sight of the HET plume.

The observed time lag in the plate current arises due to the finite ion transit times as the discharge oscillations propagate downstream. Using the data from the swept-plate configuration, it can be found that the mean beam ion exit velocity from the T-140 HET is approximately 21,700 m/s. Thus, the beam ion transit time from the HET exit plane to the axial plate is approximately 200 μs. A similar analysis for the CEX ions incident upon the radial plate yields a thermal velocity of approximately 400 m/s, with a corresponding transit time to the radial plate of 5.7 ms [35]. The sampling time in Figs. 5c and 5d is only 100 μs, and is thus too short to capture both the ion exit from the HET and its subsequent arrival at either the axial or radial plate. Thus, the oscillations in plate current in Figs. 4c and 4d are most likely due to previous discharge current oscillation cycles. This delay explains the observed differences in waveform between the captured discharge current and plate current oscillations, and it suggests that longer sampling times are required in order to capture the full lag of the plate current waveform.

For the voltage data of the floating-plate configuration and the plate-to-plate current from the connected-plate configuration, the same correlation with the discharge current is absent. This indicates that the discharge current is not the primary forcing function driving the plate-to-plate current. Rather, the nearly constant floating voltage differential that arises in the chamber due to the spatial structure of the plasma plume drives a nearly constant current between the two plates. This result again indicates that the chamber in the floating case spatially redistributes charge instead of providing a pathway for charge to ground.

Despite the observed change in collected plate current, the change from grounded to floating plates did not alter the performance or operation of the T-140 HET. Specifically, the cathode-to-ground voltage and discharge current remained constant regardless if the plates were grounded or floating. This result is not unexpected, as the Debye length in the lower-density less-energetic far-field plasma is on the order of 70 μm, which is orders of magnitude less than the spacing between the HET and the plates [24]. Thus, the bulk plasma interacting with the HET is shielded from the plates in both the grounded- and floating-plate configurations, and the HET operates independently of whether the downstream recombination of beam ions occurs due to electrons from ground or spatial charge recombination through the chamber itself.

V. Conclusions

This work explored the connection between the HET electrical circuit and the conducting walls of a vacuum test facility. Current-voltage sweeps of large aluminum plates indicate a possible coupling between the electrical properties of the test facility and the HET circuit caused by the ability of high wall biases to increase the bulk plasma potential. However, the increase in plasma potential did not cause a change in acceleration voltage. The constancy of acceleration voltage with respect to plate bias, in turn, suggests that HET performance is independent of facility bias but that the HET circuit is not. This dependence is artificially introduced by the presence of the facility and is expected to be absent on orbit.

Current measurements using grounded, aluminum plates indicate that the chamber walls serve as an active recombination pathway and that the current conducted through the grounded chamber is driven primarily by the discharge current of the HET. The collection of a significant electron current by the radial plate furthermore suggests that the vacuum facility walls provide an alternate electron path; therefore, any processes dependent upon the path of the electrons (e.g., plasma reactance and resistance) may be different between facility operation and operation in space, and thus may need to be accounted for during ground testing.

Floating the plates revealed that the directed ion beam causes a net positive floating voltage within the line of sight of the HET plume, whereas CEX ions and mobile electrons caused a negative floating voltage outside of this central region. The connected-plate configuration shows that current flows between the axial and radial wall regions. This indicates that floating conductive chamber walls allow for charge transport and serve to spatially redistribute the collected charge. As this redistribution is driven by a nearly constant spatial potential difference in the chamber, it is largely unaffected by discharge current oscillations. Further, switching from the grounded-plate to the floating-plate configuration showed no change in the discharge current or cathode-to-ground voltage, thus indicating that the plates were sufficiently far away to be shielded from the bulk plasma by sheath formation and that the HET operated independently of the wall configuration at low wall biases.

Acknowledgments

Jason Frieman is supported by the National Science Foundation Graduate Research Fellowship under grant no. DGE-1148903. The authors would like to thank Nicole Tyman for her hardware assistance and Sam Langendorf for his very helpful discussions in the preparation of this manuscript.

References

[1] Brophy, J. R., Friedman, L., and Culick, F., "Asteroid Retrieval Feasibility," *2012 IEEE Aerospace Conference*, IEEE, Piscataway, NJ, 2012, pp. 1–16. doi:10.1109/AERO.2012.618703

[2] Semenkin, A., Kim, V., Gorshkov, O., and Jankovsky, R., "Development of Electric Propulsion Standards-Current Status and Further Activity," *27th International Electric Propulsion Conference*, Electric Rocket Propulsion Society, IEPC Paper 2001-070, Fairview Park, OH, 2001.

[3] Randolph, T., Kim, V., Kaufman, H. R., Kozubsky, K., Zhurin, V. V., and Day, M., "Facility Effects on Stationary Plasma Thruster Testing," *Proceedings of the 23rd International Electric Propulsion Conference*, Electric Rocket Propulsion Society, IEPC Paper 1993-093, Fairview Park, OH, 1993.

[4] Goebel, D. M., and Katz, I., *Fundamentals of Electric Propulsion: Ion and Hall Thrusters*, Wiley, Hoboken, NJ, 2008, pp. 325–341.

[5] Hofer, R. R., Peterson, P. Y., and Gallimore, A. D., "Characterizing Vacuum Facility Backpressure Effects on the Performance of a Hall Thruster," *27th International Electric Propulsion Conference*, Electric Rocket Propulsion Society, IEPC Paper 2001-045, Fairview Park, OH, 2001.

[6] Diamant, K. D., Spektor, R., Beiting, E. J., Young, J. A., and Curtiss, T. J., "The Effects of Background Pressure on Hall Thruster Operation," *48th AIAA/ASMA/SAE/ASEE Joint Propulsion Conference and Exhibit*, AIAA Paper 2012-3735, 2012.

[7] Nakles, M. R., and Hargus, W. A., "Background Pressure Effects on Ion Velocity Distribution Within a Medium-Power Hall Thruster," *Journal of Propulsion and Power*, Vol. 27, No. 4, 2011, pp. 737–743. doi:10.2514/1.48027

[8] Brown, D. L., and Gallimore, A. D., "Evaluation of Plume Divergence and Facility Effects on Far-Field Faraday Probe Current Density Profiles," *31st International Electric Propulsion Conference*, Electric Rocket Propulsion Society, IEPC Paper 2009-030, Fairview Park, OH, 2009.

[9] Reid, B. M., "The Influence of Neutral Flow Rate in the Operation of Hall Thrusters," Ph.D. Dissertation, Aerospace Engineering Dept., Univ. of Michigan, Ann Arbor, MI, 2009, pp. 306–319.

[10] Walker, M. L. R., Hofer, R. R., and Gallimore, A. D., "The Effects of Nude Faraday Probe Design and Vacuum Facility Backpressure on the Measured Ion Current Density Profile of Hall Thruster Plumes," *38th AIAA/ASME/SAE/ASEE Joint Propulsion Conference and Exhibit*, AIAA Paper 2002-4253, 2002.

[11] Walker, M. L. R., Victor, A. L., Hofer, R. R., and Gallimore, A. D., "Effect of Backpressure on Ion Current Density Measurements in Hall Thruster Plumes," *Journal of Propulsion and Power*, Vol. 21, No. 3, 2005, pp. 408–415. doi:10.2514/1.7713

[12] Walker, M. L. R., "Effects of Facility Backpressure on the Performance and Plume of a Hall Thruster," Ph.D. Dissertation, Aerospace Engineering Dept., Univ. of Michigan, Ann Arbor, MI, 2005, pp. 126–135.

[13] Azziz, Y., Martinez-Sanchez, M., and Szabo, J. J., "Determination of In-Orbit Plume Characteristics from Laboratory Measurements," *42nd AIAA/ASME/SAE/ASEE Joint Propulsion Conference and Exhibit*, AIAA Paper 2006-4484, 2006. doi:10.2514/6.2006-4484

[14] Kieckhafer, A. W., and Walker, M. L. R., "Recirculating Liquid Nitrogen System for Operation of Cryogenic Pumps," *32nd International Electric Propulsion Conference*, Electric Rocket Propulsion Society, IEPC Paper 2011-217, Fairview Park, OH, 2011.

[15] Dushman, S., and Lafferty, J. M., *Scientific Foundations of Vacuum Technique*, Wiley, New York, 1962, pp. 349–359.

[16] McLean, C. H., McVey, J. B., and Schappell, D. T., "Testing of a U.S.-Built HET System for Orbit Transfer Applications," *35th AIAA/ASME/SAE/ASEE Joint Propulsion Conference and Exhibit*, AIAA Paper 1999-2574, 1999. doi:10.2514/6.1999-2574

[17] Sommerville, J. D., and King, L. B., "Hall-Effect Thruster–Cathode Coupling, Part II: Ion Beam and Near-Field Plume," *Journal of Propulsion and Power*, Vol. 27, No. 4, 2011, pp. 754–767. doi:10.2514/1.50124

[18] Sommerville, J. D., and King, L. B., "Hall-Effect Thruster–Cathode Coupling, Part I: Efficiency Improvements from an Extended Outer Pole," *Journal of Propulsion and Power*, Vol. 27, No. 4, 2011, pp. 744–753. doi:10.2514/1.50123

[19] Snyder, J. S., Baldwin, J., Frieman, J. D., Walker, M. L. R., Hicks, N. S., Polzin, K. A., and Singleton, J. T., "Flow Control and Measurement in Electric Propulsion Systems: Towards an AIAA Reference Standard," *33rd International Electric Propulsion Conference*, Electric Rocket Propulsion Society, IEPC Paper 2013-425, Fairview Park, OH, 2013.

[20] Xu, K. N. G., and Walker, M. L. R., "Plume Characterization of an Ion-Focusing Hall Thruster," *Journal of Propulsion and Power*, Vol. 28, No. 5, 2012, pp. 1105–1115. doi:10.2514/1.B34433

[21] Litvak, A., Raitses, Y., and Fisch, N., "Experimental Studies of High-Frequency Oscillations in Hall Thrusters," *38th AIAA/ASME/SAE/ASEE Joint Propulsion Conference and Exhibit*, AIAA Paper 2002-3825, 2002. doi:10.2514/6.2002-3825

[22] Kurzyna, J., Mazouffre, S., Lazurenko, A., Albarede, L., Bonhomme, G., Makowski, K., Dudeck, M., and Peradzynski, Z., "Spectral Analysis of Hall-Effect Thruster Plasma Oscillations Based on the Empirical Mode Decomposition," *Physics of Plasmas*, Vol. 12, No. 12, 2005, Paper 123506. doi:10.1063/1.2145020

[23] Demidov, V. I., Ratynskaia, S. V., and Rypdal, K., "Electric Probes for Plasmas: The Link Between Theory and Instrument," *Review of Scientific Instruments*, Vol. 73, No. 10, 2002, pp. 3409–3439. doi:10.1063/1.1505099

[24] Piel, A., *Plasma Physics an Introduction to Laboratory, Space, and Fusion Plasmas*, Springer–Verlag, Berlin, 2010, pp. 1411–1426.

[25] Choueiri, E. Y., "Plasma Oscillations in Hall Thrusters," *Physics of Plasmas*, Vol. 8, No. 4, 2001, pp. 1411–1426. doi:10.1063/1.1354644

[26] Litvak, A., and Fisch, N., "Rayleigh Instability in Hall Thrusters," *38th AIAA/ASME/SAE/ASEE Joint Propulsion Conference and Exhibit*, AIAA Paper 2002-3952, 2002.
doi:10.2514/6.2002-3952

[27] Zhurin, V. V., Kaufman, H. R., and Robinson, R. S., "Physics of Closed Drift Thrusters," *Plasma Sources Science and Technology*, Vol. 8, No. 1, 1999, pp. R1–R20.
doi:10.1088/0963-0252/8/1/021

[28] Manzella, D. H., and Sankovic, J. M., "Hall Thruster Ion Beam Characterization," *31st Joint Propulsion Conference and Exhibit*, AIAA Paper 1995-2927, 1995.

[29] Jahn, R. G., *Physics of Electric Propulsion*, McGraw–Hill, New York, 1968, pp. 45–68.

[30] VanGilder, D. B., Boyd, I. D., and Keidar, M., "Particle Simulations of a Hall Thruster Plume," *Journal of Spacecraft and Rockets*, Vol. 37, No. 1, 2000, pp. 129–136.
doi:10.2514/2.3536

[31] Coburn, J. W., and Kay, E., "Positive-Ion Bombardment of Substrates in Rf Diode Glow-Discharge Sputtering," *Journal of Applied Physics*, Vol. 43, No. 12, 1972, pp. 4965–4971.
doi:10.1063/1.1661054

[32] Logue, M. D., Shin, H., Zhu, W., Xu, L., Donnelly, V. M., Economou, D. J., and Kushner, M. J., "Ion Energy Distributions in Inductively Coupled Plasmas Having a Biased Boundary Electrode," *Plasma Sources Science and Technology*, Vol. 21, No. 6, 2012, Paper 065009.
doi:10.1088/0963-0252/21/6/065009

[33] Shin, H., Zhu, W., Xu, L., Donnelly, V. M., and Economou, D. J., "Control of Ion Energy Distributions Using a Pulsed Plasma with Synchronous Bias on a Boundary Electrode," *Plasma Sources Science and Technology*, Vol. 20, No. 5, 2011, Paper 055001.
doi:10.1088/0963-0252/20/5/055001

[34] McDonald, M. S., and Gallimore, A. D., "Cathode Position and Orientation Effects on Cathode Coupling in a 6-kW Hall Thruster," *31st International Electric Propulsion Conference*, Electric Rocket Propulsion Society, IEPC Paper 2009-113, Fairview Park, OH, 2009.

[35] Boyd, I. D., and Dressler, R. A., "Far Field Modeling of the Plasma Plume of a Hall Thruster," *Journal of Applied Physics*, Vol. 92, No. 4, 2002, pp. 1764–1774.
doi:10.1063/1.1492014

J. Blandino
Associate Editor